RSC Advances

PAPER

View Article Online
View Journal | View Issue

Cite this: *RSC Adv.*, 2022, **12**, 10005

pH-responsive curcumin-based nanoscale ZIF-8 combining chemophotodynamic therapy for excellent antibacterial activity†

Xiaofeng Meng,‡[ab] Jingwei Guan,‡[ab] Shanshan Lai,[ab] Liming Fang*[cef] and Jianyu Su *[abcd]

Received 30th December 2021
Accepted 2nd March 2022

DOI: 10.1039/d1ra09450e

rsc.li/rsc-advances

Antimicrobial photodynamic therapy (aPDT) is a highly attractive therapy due to its advantages of being a non-antibiotic procedure for reducing drug-resistant microbes. Curcumin (CCM) has been considered as a natural photosensitizer for PDT with prominent antibacterial, antifungal, and anti-proliferative activity. However, its excellent biological and pharmacological activities are limited because of its low solubility, rapid metabolization and instability. Herein, we reported a promising agent based on CCM-incorporated into zeolitic imidazolate framework-8 (ZIF@CCM). The as-prepared nanoparticle exhibited high drug loading capability (11.57%) and drug loading encapsulation (82.76%). Additionally, ZIF@CCM displayed a pH-responsive drug release behavior and chemophotodynamic therapy for excellent antibacterial activity. The underlying mechanism elucidated that Zn^{2+} released from ZIF-8 increased the permeability of the bacterial cell membrane with leakages of K^{+}. The overproduction of extracellular ROS further resulted in the disrupted bacterial cell membrane and distorted bacterial morphology. Thus, ZIF@CCM-mediated photodynamic activation might be a promising treatment strategy for microbial inactivation.

1. Introduction

Bacterial infection has become one of the biggest global health problems, leading to great negative impacts on medical and health care.[1] The misuse and overuse of antibiotics had resulted in the rapid emergence of drug-resistant bacteria.[2] Therefore, the development of new effective antimicrobial strategies without using antibiotics turns into an urgent task. Recently, antimicrobial photodynamic therapy (aPDT) as a non-antibiotic therapy has gained rapid acceptance in the treatment of bacterial infection.[3] The bacteriostatic mechanism of aPDT might be attributed to the production of reactive oxygen species (ROS) by a photosensitizer under the conditions of adequate light irradiation.[4] ROS could react with the bacterial components like their cell wall and cell membrane and alter the structure chemically. High levels of these species may result into lipid peroxidation, protein oxidation, DNA degradation, and irreversible cell damage.[5,6] Moreover, aPDT exhibited multi-target destruction process without requiring a specific target.[7] Thus, aPDT could be effective against bacteria and reduce the risk of drug resistance.[8,9] To date, the application of aPDT has attracted increasing attention in variable food matrices, such as bean products, vegetables, and bread.[10]

Curcumin (CCM), a fluorescence polyphenolic compound, is regarded as an effective natural photosensitizer due to the maximum absorption wavelength near blue light (455–460 nm).[11] It has been conformed to possess broad-spectrum biological and pharmacological activities, including anti-inflammatory, phototoxicity, antitumor and antibacterial properties.[12,13] Unfortunately, the bioavailability of CCM was limited due to the intrinsic physicochemical properties such as the low solubility in water, the poor photostability and thermal stability.[13,14] Besides, the negatively charged state made it difficult to contact and adhere to the surface of negatively charged bacteria.[7] To circumvent the problem, an ideal nano-carrier for CCM has been explored widely.

Zeolitic imidazolate framework 8 (ZIF-8), a representative subclass of metal–organic frameworks (MOFs), was constructed by Zn^{2+} ions and 2-methylimidazole.[15] Previous studies revealed that ZIF-8 possessing fantastic thermal and chemical stability was of

[a]*School of Food Science and Engineering, South China University of Technology, Guangzhou 510640, Guangdong, China. E-mail: jysu@scut.edu.cn*

[b]*Guangdong Province Key Laboratory for Green Processing of Natural Products and Product Safety, Guangzhou, 510640, Guangdong, China*

[c]*Sino-Singapore International Joint Research Institute, Guangzhou 510700, Guangdong, China*

[d]*Overseas Expertise Introduction Center for Discipline Innovation of Food Nutrition and Human Health (111 Center), Guangzhou 510640, Guangdong, China*

[e]*Key Laboratory of Biomedical Engineering of Guangdong Province, School of Materials Science and Engineering, South China University of Technology, Guangzhou 510640, China*

[f]*National Engineering Research Center for Tissue Restoration and Reconstruction, South China University of Technology, Guangzhou 510006, China*

† Electronic supplementary information (ESI) available. See DOI: 10.1039/d1ra09450e

‡ These authors contributed equally to this work.

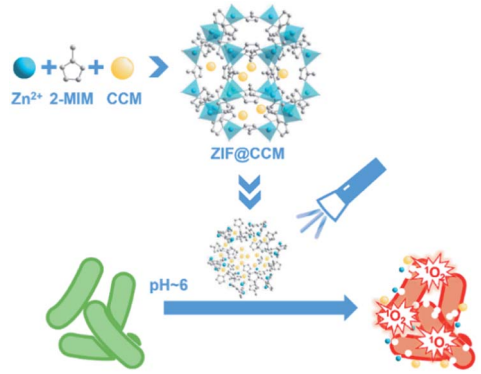

Scheme 1 Schematic illustration of the preparation of ZIF@CCM and its application for photodynamic antibacterial response.

great popularity for drug encapsulation such as doxorubicin hydrochloride, lysozyme, and rapamycin.[16,17] Due to the unique porous structure, adjustable particle size and variable chemical surface, ZIF-8 could encapsulate plentiful CCM to form CCM-loaded ZIF-8 nanoparticles (ZIF@CCM) for aPDT. ZIF@CCM exhibited the excellent stability in physiological environment while performed pH-sensitive release property in bacterial micro-acid environment.[16] CCM released from ZIF@CCM could perform inhibition effects on bacterial growth and further enhance the bactericidal activity of photodynamic treatment.[18] Besides, Zn^{2+} ions released from ZIF-8 also blocked the bacterial growth and exhibited good anti-inflammation effect.[15] On the other hand, the positively charged metal sites of architecturally structure increased the interaction with the bacterial surface and destroyed the bacterial membrane, thereby enhancing the photodynamic germicidal efficacy.[19]

Herein, a pH-responsive core–shell nanocomposite (ZIF@CCM) was successfully fabricated (Scheme 1). The shapes and crystalline structures of as-prepared ZIF@CCM were verified with different microscopic and spectroscopic measurements, such as scanning electron microscope (SEM), Fourier transform infrared (FT-IR), UV-vis spectroscopy and Zetasizer Nano-ZS. CCM incorporation into ZIF@CCM exhibited good stability and greatly improved the water solubility. More importantly, minimal inhibitory concentration (MIC) and minimal bactericidal concentration (MBC) assays demonstrated that blue light-activated ZIF@CCM significantly blocked the bacterial growth. To further investigate the underlying mechanism of ZIF@CCM-mediated photodynamic activation, ROS generation and K^+ ion leakage were measured. Taken together, the aPDT of ZIF@CCM exhibited a prominent bactericidal activity against *E. coli* and *S. aureus*, revealing the potential application in microbial eradication.

2. Results and discussion, experimental

2.1. Design and characterization of ZIF@CCM

CCM-loaded ZIF-8 was fabricated as illustrated in Scheme 1. ZIF@CCM nanoparticles were prepared based on a single-step procedure. The concentration of CCM and reaction time during the synthesis procedure were optimized to initiate the efficient photodynamic treatment. The optimal ZIF@CCM was prepared by selecting 5 mg mL^{-1} of CCM and reacting for 5 min, based on UV-vis spectra (Fig. S1†), with the corresponding drug loading capability (DLC) and drug loading encapsulation (DLE) verified as 11.57% and 82.76%, respectively (Table S1†).

The shape and size of as-prepared ZIF-8 and ZIF@CCM were shown in Fig. 1. The hydrodynamic sizes of ZIF@CCM and ZIF-8 were 190.43 nm and 112.27 nm, respectively. Moreover, SEM images exhibited that ZIF@CCM presented uniformly in the regular dodecahedral crystals with an average diameter of 150 nm, which was larger than that of ZIF-8 with 80 nm due to the growth process of ZIF-8 influenced by CCM.[20] Then, the chemical composition and structure of ZIF@CCM were determined according to optical properties. The UV-vis was performed to confirm the successful incorporation of CCM into the ZIF-8. As depicted in the UV-vis spectrum, a strong absorbance of ZIF@CCM was present at 475 nm, which was about 50 nm red-shifted to that of CCM (Fig. 2A), revealing that CCM was encapsulated into the ZIF-8 framework. Additionally, photoluminescence (PL) was performed to analyze purity and crystalline quality. The PL spectrum were performed based on CCM with robust fluorescence emission peaked at 545 nm when it was excited at 420 nm.[21] The PL spectrum analysis showed that the emission peak of ZIF@CCM was present at 625 nm, which was 80 nm red-shifted compared to that of CCM (Fig. 2B), further conforming that CCM was incorporated into ZIF-8. Similar results have also been reported by Y. Wang *et al.*[22] The red shift appeared in UV-vis and PL spectrum might be attributed to the decreased band gap between π–π* electronic transition of CCM based on the interaction of CCM and Zn^{2+}.[22] Powder X-ray diffraction (XRD) characterization was employed to measure the phase and structural information on nanoparticles. As shown in Fig. 2C, ZIF@CCM and ZIF-8 displayed the similar crystalline characteristic diffraction peaks in XRD patterns analysis, indicating that CCM did not affect the crystal structure of ZIF-8. Besides, the absorption peaks at ~1521 cm^{-1} in the FT-IR spectra of ZIF@CCM were attributed to CCM,

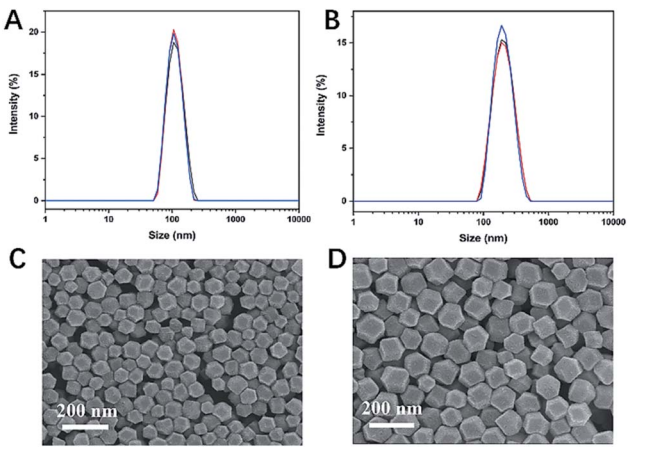

Fig. 1 Hydrodynamic sizes of ZIF-8 (A) and ZIF@CCM (B). SEM images of ZIF-8 (C) and ZIF@CCM (D).

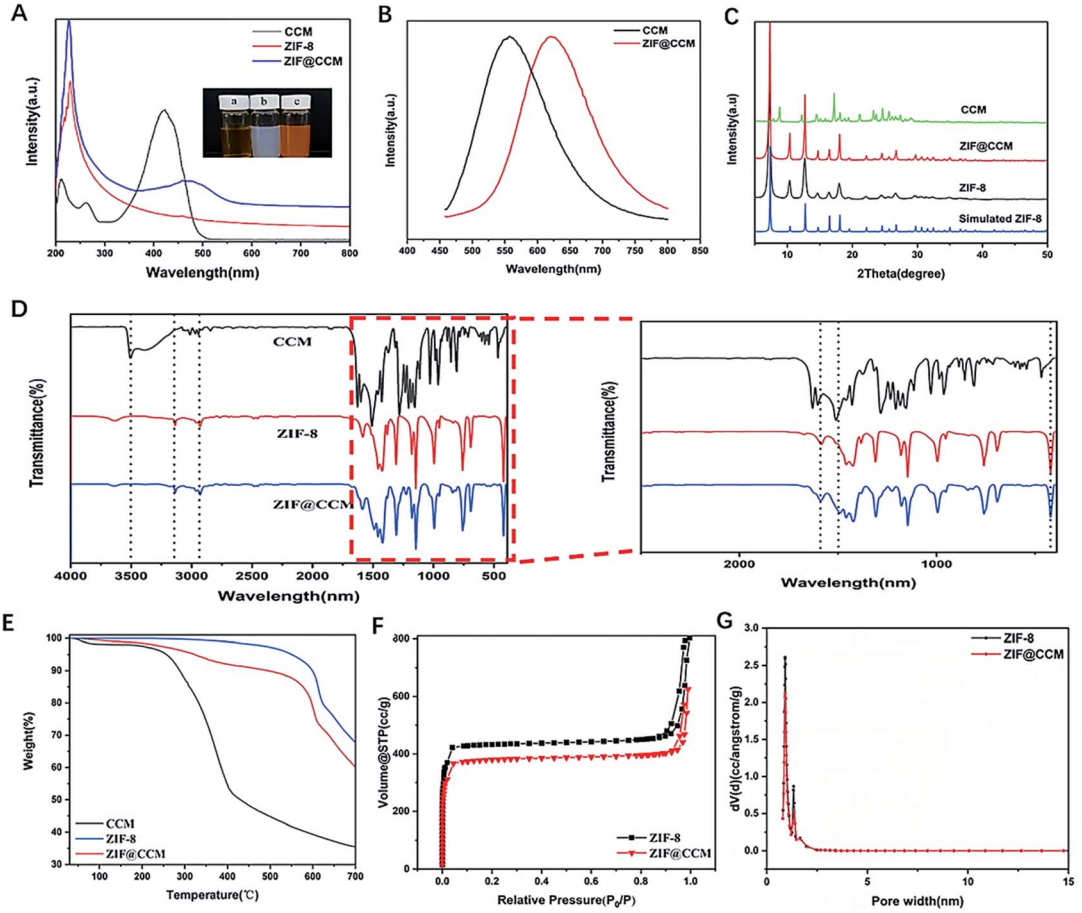

Fig. 2 Chemical composition and structure characterizations of ZIF@CCM. (A) UV-vis of the CCM, ZIF-8 and ZIF@CCM. (B) PL spectra of CCM and ZIF@CCM under the excitation of blue light. (C) XRD patterns of simulated ZIF-8, ZIF-8, ZIF@CCM and CCM. (D) FT-IR spectrum of CCM, ZIF-8 and ZIF@CCM. (E) TGA results of CCM, ZIF-8 and ZIF@CCM. (F) N^2 adsorption–desorption isotherm of ZIF@CCM and ZIF-8. (G) Pore-size distributions of ZIF-8 and ZIF@CCM.

whereas the characteristic infrared absorption peak at ~3511.7 cm^{-1} of phenolic group in ZIF@CCM was not present compared to that of CCM (Fig. 2D), verifying that the incorporation of CCM was mainly attributed to the interaction of CCM and ZIF-8.

The thermal stability of the material was determined by the thermogravimetric analysis (TGA). As shown in Fig. 2E, slight losses of mass (3–5%) were observed in CCM and ZIF@CCM below 200 °C, which were attributed to the evaporation of adsorbed water. ZIF-8 had a long plateau before 580 °C, and the high thermal stability matched well with the reported literature.[23] While ZIF@CCM showed a gradual weight loss at 250 °C, which was ascribed to a decomposition step of CCM with a strong weight loss at 200 °C. The weight loss percentage of ZIF@CCM was consistent with the results determined by UV-vis drug loading estimation (DLC%). Due to the disintegration of ZIF-8 structure in higher temperature, ZIF@CCM also exhibited some weight loss at 580 °C. Results indicated that the encapsulation of CCM did not affect the thermal stability of ZIF-8 on the ZIF@CCM structure. To verify the quantitative information about the structure of porous materials, N^2 absorption and desorption were investigated. As depicted in Fig. 2F and G, the BET surface area and pore diameter of ZIF-8 were determined as 1.5 nm and 1739.4 $m^2\ g^{-1}$, respectively, which could be conducive to incorporate CCM into the ZIF-8.

2.2. Stability and pH-sensitive of ZIF@CCM nanoparticle

The pH stability of ZIF@CCM was evaluated by release behavior of CCM from ZIF@CCM. As depicted in Fig. 3A, the retention rates of CCM incorporated ZIF@CCM were 93.38%, 96.19%, 93.01% at pH 7.4, 9 and 10 within 72 h, respectively. These results demonstrated that ZIF-8 was an effective and promising drug delivery carrier to improve the stability of CCM. Additionally, the pH-sensitive release of CCM from ZIF@CCM was also investigated. As Fig. 3B illustrated, the pH of 5.5 and 6.5 solutions stimulated a burst release of CCM from ZIF@CCM in the initial 8 h with cumulative release up to 60% and 70%, respectively. Simultaneously, Zn^{2+} released from ZIF@CCM increased as the pH values of PBS solution decreased (Fig. 3C). These results were attributed to the fact that ZIF-8 would be easily disintegrated to release the encapsulated drug upon the pH stimulus,[16] indicating that ZIF@CCM possessed a good pH-responsive release behavior.

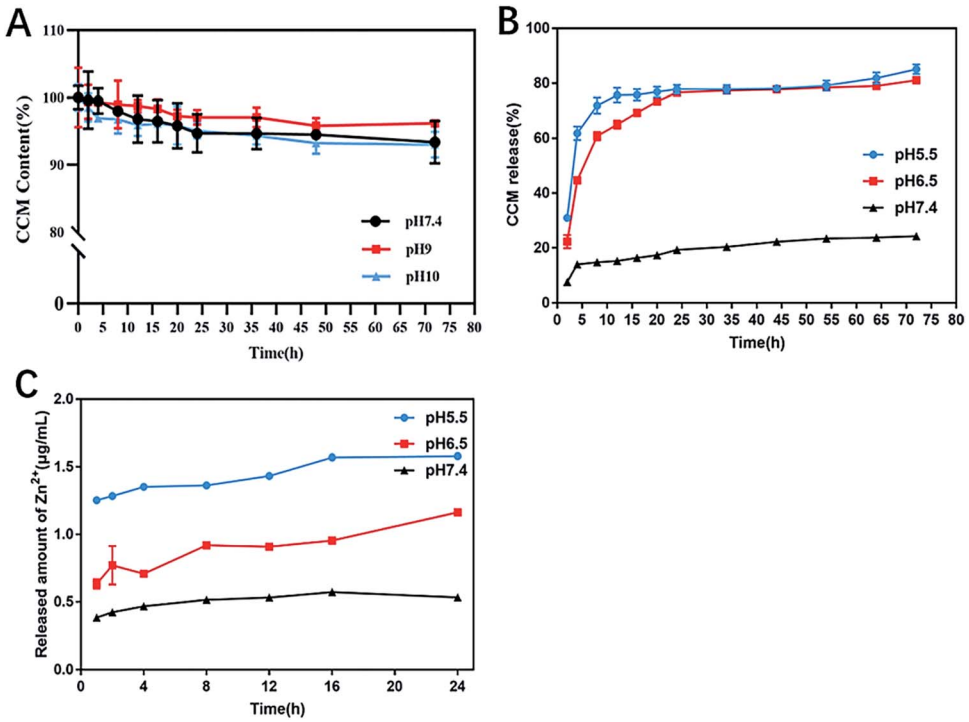

Fig. 3 (A) Stability of ZIF@CCM in different pH solutions (pH 7.4, pH 9, pH 10). (B) CCM release from ZIF@CCM in PBS solution (pH 5.5, pH 6.5 and 7.4) containing 0.5 wt% of Tween-20. (C) Zn^{2+} release from ZIF@CCM in PBS solution (pH 5.5, pH 6.5 and 7.4).

2.3. Antibacterial efficacy evaluation

To investigate the bacteriostatic effects of chemophotodynamic therapy of ZIF@CCM against *S. aureus* and *E. coli* strains, MIC, MBC and bacterial viability were evaluated. As depicted in Fig. 4, when *E. coli* and *S. aureus* strains were cotreated with ZIF-8 and blue light irradiation, no significant changes in MIC and MBC values were observed compared to that treated with ZIF-8 alone, showing that blue light irradiation had no effect on the antibacterial ability of ZIF-8. The MIC and MBC values of ZIF@CCM combined with blue light irradiation against *E. coli* were 31.25 μg mL^{-1} (containing CCM 3.59 μg mL^{-1}) and 125 μg mL^{-1} (containing CCM 14.38 μg mL^{-1}), respectively, which was significantly lower than that of ZIF@CCM alone. Besides, compared with ZIF@CCM alone, the cotreatment with ZIF@CCM and blue light irradiation against *S. aureus* exhibited a significant antibacterial effect, with MIC and MBC values of 125 μg mL^{-1} and 250 μg mL^{-1}, respectively. These results confirmed that the antibacterial activity of ZIF@CCM was enhanced in the presence of blue light irradiation. Based on the above results, 125 μg mL^{-1} and 250 μg mL^{-1} of ZIF@CCM were chosen for *E. coli* and *S. aureus* strains respectively for the subsequent experiments.

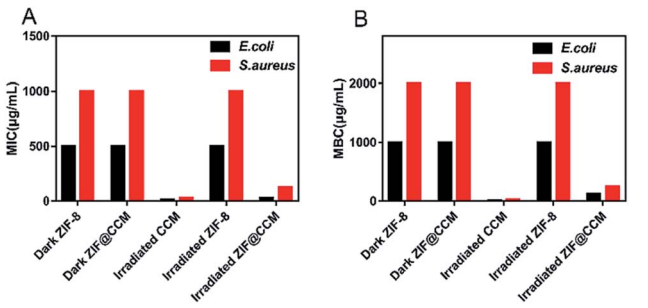

Fig. 4 MIC (A) and MBC (B) values of CCM, ZIF-8, and ZIF@CCM with blue light irradiation and dark against *E. coli* and *S. aureus*.

In addition, the bacterial survival rates of *E. coli* and *S. aureus* strains cotreated with nanoparticles and blue light irradiation were quantified (Fig. 5). No significant difference in survival rates against *S. aureus* and *E. coli* were observed in blue light irradiation alone and CCM treatment alone compared with that in the control, respectively. In contrast, the bacterial survival rate markedly decreased in the treatment of blue light irradiation in combination with ZIF@CCM and CCM compared with that in the treatment of ZIF@CCM and CCM, respectively, suggesting that blue light irradiation could trigger the aPDT of ZIF@CCM and CCM. Some studies also showed that blue light-activated CCM exhibited the promising antibacterial effect against *Helicobacter pylori*.[18] Moreover, the survival rate of ZIF@CCM-mediated photodynamic activation against *E. coli* and *S. aureus* strains was lower than that of CCM-mediated photodynamic activation, indicating that ZIF@CCM under blue light had a stronger bactericidal activity than CCM under blue light. Similar results showed that blue light-activated CCM displayed a remarkable antibacterial activity against *Shigella flexneri*, *E. coli* and *S. aureus*.[24,25] Besides, as depicted in Fig. 5C–F, colony counts of blue light-activated ZIF@CCM against *E. coli* and *S. aureus* strains obviously decreased compared with that of blue light-activated CCM, further demonstrating that ZIF@CCM-mediated photodynamic therapy exhibited the prominent bacteriostatic effects.

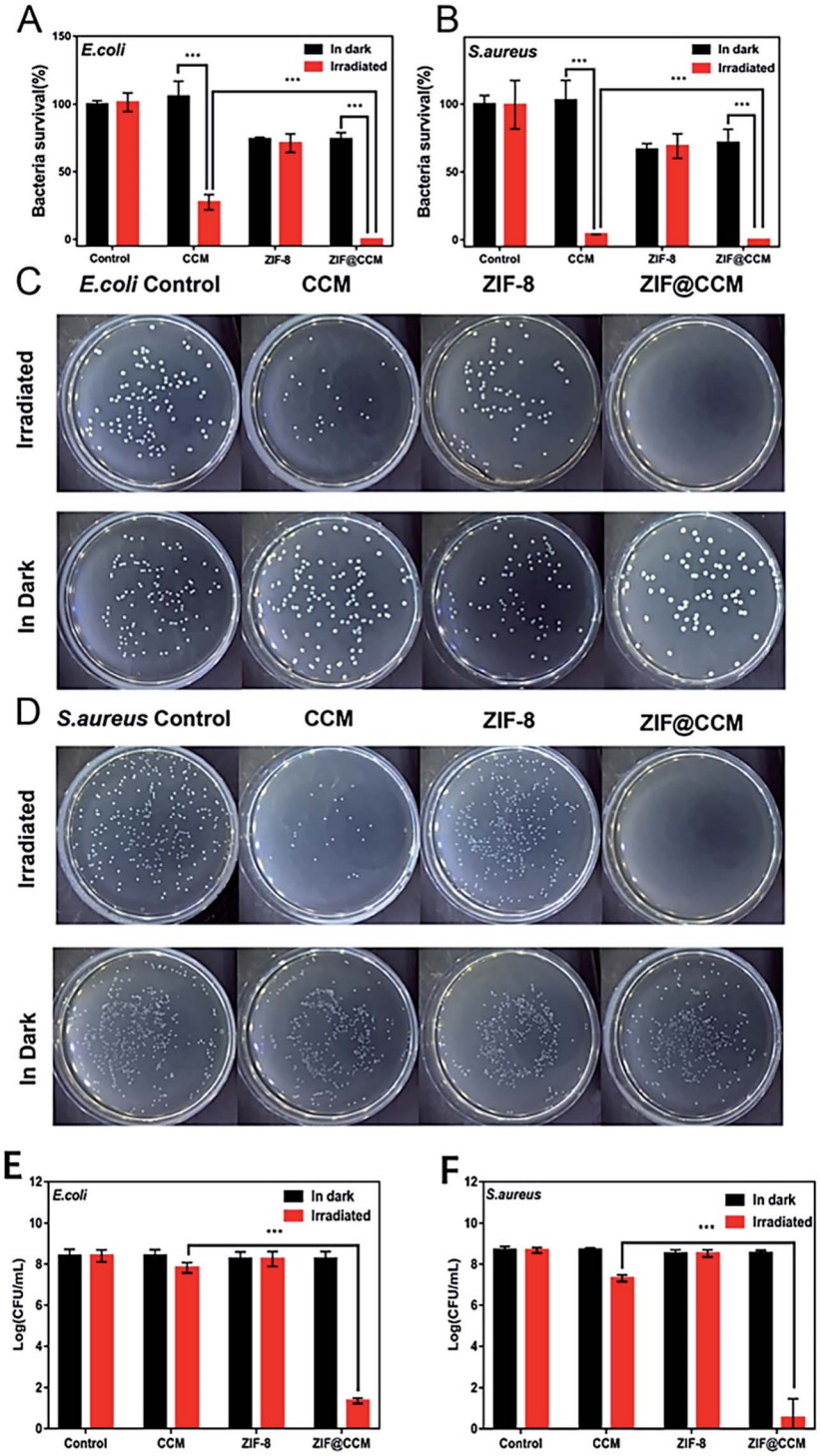

Fig. 5 The bacterial survival rate after logarithmic of *E. coli* (A) and *S. aureus* (B) cotreatment with CCM, ZIF-8 and ZIF@CCM and irradiated blue light and dark. Photographs of *E. coli* (C) and *S. aureus* (D) colonies on LB agar plates cotreated with CCM, ZIF-8 and ZIF@CCM and irradiated blue light and dark. Colony count of CCM, ZIF-8 and ZIF@CCM combined with irradiated blue light and dark against *E. coli* (E) and *S. aureus* (F).

2.4. Antibacterial mechanism study

Based on the characteristics that SYTO 9 and PI can stain living and damaged bacteria, respectively, *S. aureus* and *E. coli* strains were stained post-cotreated with nanoparticles and blue light irradiation. The representative staining images of *E. coli* and *S. aureus* were exhibited in Fig. 6. The cotreatment with blue light irradiation and CCM and ZIF@CCM exhibited high proportion of cell damage with red fluorescence present compared to CCM alone and ZIF@CCM alone, respectively, suggesting that ZIF@CCM-mediated photodynamic activation could cause highly effective microbial damage. The phototoxicity of CCM blocked bacterial growth by the autoxidation mechanism of CCM.[25,26] Light

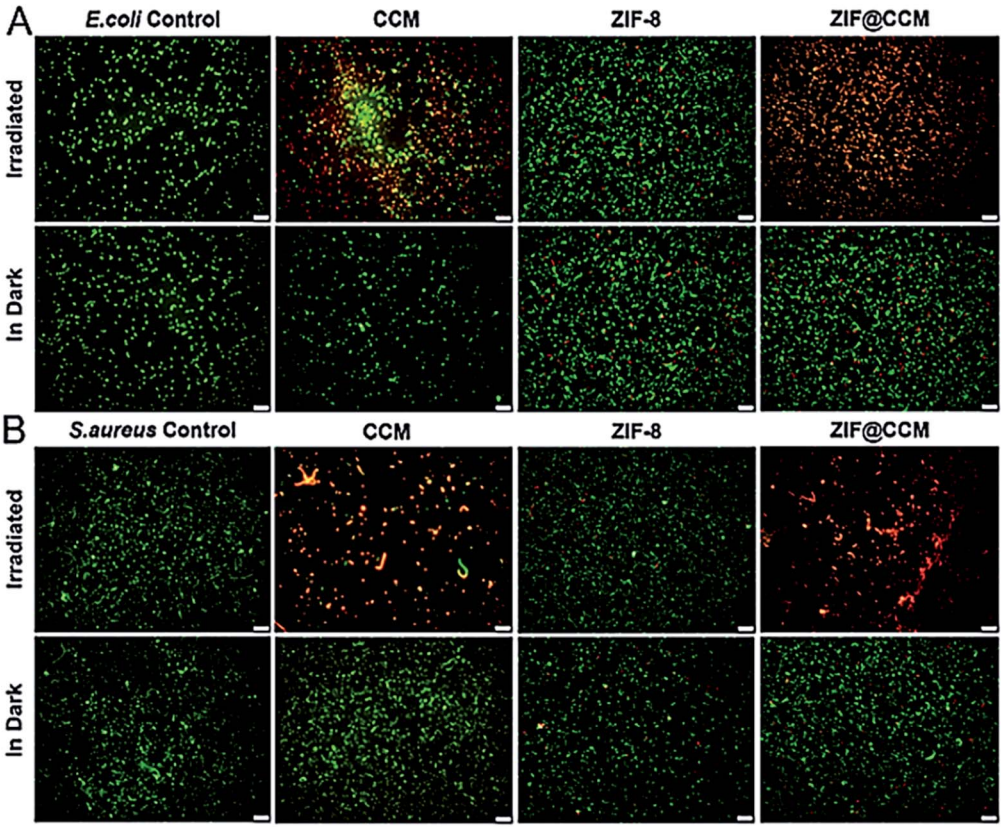

Fig. 6 Fluorescence microscope images of CCM, ZIF-8 and ZIF@CCM combined with irradiated blue light and dark against *E. coli* (A) and *S. aureus* (B). Scale bars: 50 μm.

irradiation could activate photosensitizers to induce reactive oxygen species (ROS), including singlet oxygen and superoxide.[12] ROS could result into bacterial death by oxidizing components of cell membrane and guanosine in DNA and RNA.[27,28] Therefore, indocyanine green (ICG) was applied to evaluate ROS generation after each treatment. As shown in Fig. 7A, the OD values of CCM and ZIF@CCM combined with blue light irradiation rapidly decreased to 12.80% and 7.56%, respectively. ZIF@CCM with positively charged metal sites could be electrostatically adsorbed to the bacterial surface and release CCM in bacterial micro-acid environment.[16] Therefore, $^1O_2$ was induced by CCM triggered with blue light irradiation, resulting in bacterial death.[28] Due to the spontaneous degradation of ICG under blue light, the OD value decreased in ICG and ZIF-8 group with irradiation.

To further evaluate the adverse effect of phototoxicity of ZIF@CCM on cell membrane permeability, the leakage of K^+ in the solution was quantified. As shown in Fig. 7B, the concentration of K^+ was the highest when *S. aureus* and *E. coli* strains were cotreated with ZIF@CCM and blue light irradiation, followed by strains cotreated with CCM and irradiation, demonstrating that ZIF@CCM-mediated photodynamic activation could obviously change cell membrane permeability to release of intracellular K^+ into the extracellular. This result might be attributed to the fact that Zn^{2+} released from the nanoparticles could increase the permeability of bacterial cell membrane.[15] On the other hand, the

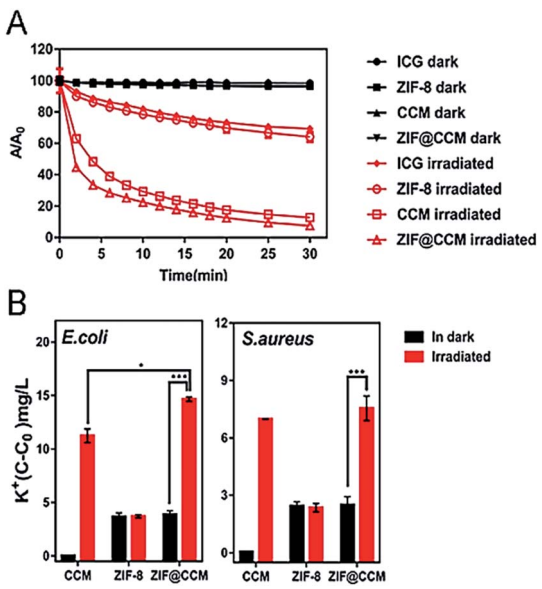

Fig. 7 (A) The degradation rate of ICG, ICG + CCM, ICG + ZIF-8 and ICG + ZIF@CCM, with blue light irradiation and dark, respectively. (B) Leakage of K^+ from *E. coli* and *S. aureus* cells treated with CCM, ZIF-8 and ZIF@CCM with irradiated blue light and dark.

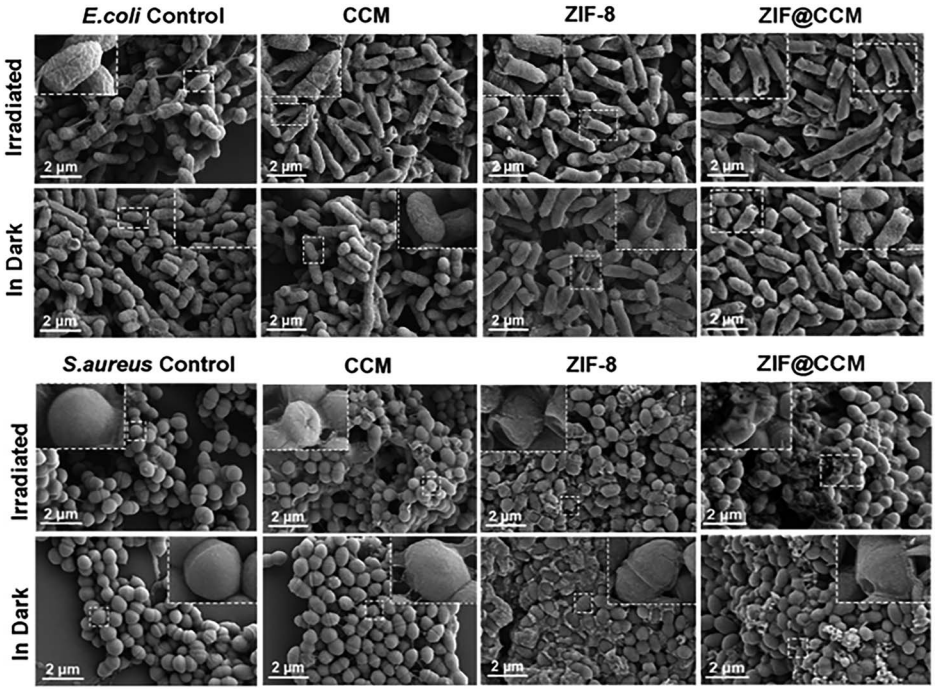

Fig. 8 The morphology of *E. coli* and *S. aureus* cells cotreated with ZIF@CCM and blue light irradiation and dark by SEM.

increased ROS induced by blue light-activated ZIF@CCM could damage the cell membrane integrity by oxidize the lipid in the membrane.[28]

Besides, bacterial morphology of *S. aureus* and *E. coli* strains were obtained by SEM to investigate the cotreatments-induced morphologic changes. Fig. 8 showed that the cotreatment with CCM and blue light against *S. aureus* and *E. coli* strains led to irreversible cell damage in the microbial cells. Punctured and deformed cells with compromised cell integrity (evidence of intracellular leakage) were more prominently observed in ZIF@CCM compared to CCM and ZIF-8 alone. Photogenerated extracellular ROS by CCM, ZIF-8, and ZIF@CCM was presumably sufficient to cause bacterial cell wall damage, including compromised cell membrane integrity, and decomposition of the cell envelope.[29] Similar observations have been reported in the literature for dead cells.[30–33]

3. Conclusions

In the present study, a nano-antibacterial agent based on CCM and ZIF-8 was successfully fabricated for aPDT. ZIF@CCM exhibited the high CCM-loading capacity, the long-term stability, and the improved bioavailability. Additionally, CCM released from ZIE@CCM under blue light irradiation induced the significant antibacterial effects by the overproduction of extracellular ROS and destroying the bacterial cell membrane. At the same time, the released Zn^{2+} synergistically acted as bactericidal activity. Our studies proved that ZIF@CCM combining chemophotodynamic therapy might be a rapid and effective strategy for microbial eradication.

4. Materials and methods

4.1. Materials

Zinc nitrate hexahydrate ($ZnNO_3 \cdot 6H_2O$, 99%), ethanol (CH_3CH_3O, 99.7%) and methanol (CH_3OH, 99.5%) were purchased from Guang Zhou Chemical Reagent Factory. 2-Methylimidazole (2-MIM, 98%) was purchased from Macklin. Curcumin (CCM, 98%) and indocyanine green (ICG, 75%) were purchased from Aladdin. Bacterial culture media was purchased from Huan Kai Microbial. Gram-positive bacteria (*S. aureus*, ATCC 23235) and Gram-negative bacteria (*E. coli*, ATCC 43894) were obtained from China Center of Industrial Culture. LIVE/DEAD Bac Light Bacterial Viability Kit was purchased from Thermo Fisher Scientific.

4.2. Synthesis of ZIF@CCM

CCM-loaded ZIF-8 was synthesized in one step method as previously described.[25,34] In brief, a stock solution of 30 mg mL^{-1} $ZnNO_3 \cdot 6H_2O$ was prepared freshly. Subsequently, 5 mL $ZnNO_3 \cdot 6H_2O$ stock solution was added into 10 mL of methanol-dispersed 2-methyl imidazole (330 mg) and CCM (5 mg) with sonication for 10 min. Then, the mixture was centrifuged at 10 000 rpm for 30 min and rinsed with methanol for 3 times. Finally, the purification was dried under vacuum at 25 °C for 24 h.

4.3. Quantification of CCM incorporation into ZIF@CCM

The total amount of CCM encapsulation into ZIF@CCM was determined by UV-vis spectrophotometer (BioDrop TOUCH

Duo). The as-prepared ZIF@CCM was mixed with hydrochloric acid (50 μL) and absolute ethanol (9.95 mL) and sonicated for 10 min to extract CCM from ZIF@CCM. The absorbance at 425 nm (Abs_{425}) of the above solution was measured. The concentration of CCM was determined based on a calibration curve established with different amounts of CCM dissolved in absolute ethanol. The percent of DLC and DLE were calculated according to following equations:

$$\text{DLE } (\%) = \frac{\text{Encapsulated CCM (mg)}}{\text{Total CCM input (mg)}} \times 100\%$$

$$\text{DLC } (\%) = \frac{\text{Encapsulated CCM (mg)}}{\text{Total composite nanoparticles (mg)}} \times 100\%$$

4.4. Characterization of ZIF@CCM

The crystalline structure of the as-prepared nanoparticle was carried out on a powder X-ray diffraction (XRD) system (Bruker D8 ADVANCE, Germany) with Cu Kα ($\lambda = 1.5418$ Å) radiation source in the range of 5–50° (2θ). The SEM images of nanoparticles were visualized by SEM microscope (SEM, Zeiss Merlin) with a thin film on a silicon chip. Chemical composition of the nanoparticles was measured by FT-IR using infrared spectrometer (Bruker VERTEX 70). Zetasizer Nano-ZS (Malvern Instruments, Malvern, UK) was used to obtain size distribution and PDI. The Brunuer–Emmett–Teller (BET) surface area measurements were performed on Micromeritics ASAP 2460, automatic volumetric instrument with nitrogen adsorption measurements. The thermal properties of nanoparticles were measured by simultaneous thermal analyzer (TGA, NETZSCH STA449 F3), with analyzer under nitrogen atmosphere from 25 °C to 700 °C at accelerating rate of 5 °C min^{-1}. Fluorescent emission spectrum was recorded using a fluorescence spectrophotometer with excitation at 425 nm (TECAN Infinite M200 Pro NanoQuant).

4.5. *In Vitro* stability of ZIF@CCM

ZIF@CCM was dispersed into 1 mL of PBS (pH 7.4, pH 9 and pH 10), separately. The solutions of ZIF@CCM were centrifugated and digested by 100 μL hydrochloric acid (2 M) at specific intervals. Then the amount of residual CCM from ZIF@CCM system dissolved with ethanol were measured as described in Section 4.3. Accordingly, the cumulative amount of CCM released from ZIF@CCM system was determined.

4.6. *In vitro* CCM and Zn^{2+} ions release from ZIF@CCM system

ZIF@CCM (10 mg) was dissolved in 20 mL of phosphate buffered saline (PBS, pH 7.4, pH 6.5 and pH 5.5) containing Tween-20 (0.5 wt%) with constantly shaking. At specific intervals, 1 mL of buffer solution outside the dialysis bag was taken out and equal volume of fresh buffer was replenished. The released amount of CCM was determined by UV-vis spectrophotometer.

The release behavior of Zn^{2+} ions from ZIF@CCM system was analyzed by suspending 20 mg of ZIF@CCM into 20 mL of PBS (pH 7.4, pH 6.5 and pH 5.5). 1 mL of buffer solution was obtained at the same method above. Then the concentration of Zn^{2+} ions in the solution were determined by atomic absorption spectrometer (HITACHI Z-2000).

4.7. Analysis of ROS generation by ZIF@CCM combined with blue light

ICG was chosen as a singlet oxygen probe.[35] The stock of ICG (1 mg mL^{-1}) diluted with distilled water was mixed with ZIF@CCM, CCM and ZIF-8 suspension in 96-well plates, respectively. After irradiation with blue light, the ROS level at specific intervals was determined by microplate spectrophotometer at 780 nm.

4.8. Photodynamic inactivation of bacteria by ZIF@CCM

The aPDT of ZIF@CCM against *E. coli* (ATCC43894) and *S. aureus* (ATCC23235) were determined by colony count, MIC and MBC based on a modified broth microdilution method. Briefly, the double dilution method was used to obtain the final concentration of ZIF@CCM range from 7.8125 to 4000 μg mL^{-1}. Subsequently, 100 μL of pretreated microbial suspensions were incubated with ZIF@CCM at 37 °C for 1 h. After irradiation under blue light (420–430 nm) with 2.2 mW cm^{-2} measured by an survival rate (TES1332A, Taiwan, China) for 1 h, the microbial suspensions were cultured at 37 °C for 22 h and shaken at 200 rpm. To the end, the optical density (OD) of the microbial suspensions at 600 nm (OD_{600}) were determined by a microplate reader (Tecan Trading Co., Ltd, Switzerland). MBC was the lowest concentration without visible bacterial growth after incubating illuminated 100 μL subculture from each well on agar plates at 37 °C for 24 h. Single colonies of each type of bacteria were cultured in the LB medium. All tests were performed in triplicate.

4.9. Intracellular K^+ ion leakage

After cotreatment with ZIF@CCM and blue light irradiation, the bacterial suspensions were harvested and centrifuged. The concentration of K^+ ion in the LB supernatant was measured by atomic absorption spectrometry.

4.10. Morphology of bacteria

The bacteria cotreated with nanoparticles and blue light irradiation were collected, followed by being washed with PBS and fixed with a 2.5% glutaraldehyde solution at 4 °C for 24 h. After dehydration in graded alcohol solutions, the bacteria were inoculated onto silicon wafers. Then the silicon wafers were sprayed with gold and finally visualized by SEM imaging.

4.11. Statistical analysis

All experiments were carried out in triplicate, and results were expressed as mean ± standard deviation (SD). Statistical analysis was performed by using SPSS statistical program version 20.0 (IBM Corp., Armonk, NY, USA). Difference between two

groups was analyzed by two-tailed Student's *t*-test. Differences with $*p < 0.05$, $**p < 0.01$, or $***p < 0.001$ were considered statistically significant. Differences among multiple groups were analyzed using one-way analysis of variance (ANOVA) with Tukey's test.

Author contributions

Xiaofeng Meng: designed and performed the experiments, methodology, and writing-review & editing. Jingwei Guan: conceptualization, development, performed experiments and writing-original draft. Shanshan Lai: software, conceptualization and methodology. Jianyu Su: supervision, conceptualization, writing-review & editing. Liming Fang: supervision, investigation, writing-review & editing.

Conflicts of interest

The authors declare no conflict of interest.

Acknowledgements

This work was supported by the National Key Research and Development Program of China (2017YFD0601303), the Science and Technology Planning Project of Guangdong Province (2019A1515011891, 2020A1414010360, 2015A030312004), the Science and Technology Program of Guangzhou (201903010025), the Tip-top Scientific and Technical Innovative Youth Talents of Guangdong Special Support Program (2019TQ05N359), and the Fundamental Research Funds for the Central Universities (2020ZYGXZR062), SCUT.

References

1 Q. Zhang, G. Lambert, D. Liao, H. Kim, K. Robin, C. K. Tung, N. Pourmand and R. H. Austin, *Science*, 2011, **333**, 1764–1767.
2 X. Li, H. Bai, Y. Yang, J. Yoon, S. Wang and X. Zhang, *Adv. Mater.*, 2019, **31**, 1805091–1805092.
3 X. Wen, X. Zhang, G. Szewczyk, A. El-Hussein, Y. Y. Huang, T. Sarna and M. R. Hamblin, *Antimicrob. Agents Chemother.*, 2017, **61**, 417–467.
4 Y. Jiang, A. W. Leung, H. Hua, X. Rao and C. Xu, *Int. J. Photoenergy*, 2014, **2014**, 11054–11066.
5 P. K. Samantaray, G. Madras and S. Bose, *Adv. Sustainable Syst.*, 2019, **3**, 1900017.
6 R. Canaparo, F. Foglietta, T. Limongi and L. Serpe, *Materials*, 2020, **14**, 53.
7 M. R. Agel, E. Baghdan, S. R. Pinnapireddy, J. Lehmann, J. Schafer and U. Bakowsky, *Colloids Surf., B*, 2019, **178**, 460–468.
8 M. R. Hamblin, *Curr. Opin. Microbiol.*, 2016, **33**, 67–73.
9 X. J. Fu, Y. Fang and M. Yao, *BioMed Res. Int.*, 2013, **2013**, 159157.
10 L. D. Prado-Silva, G. Brancini, G. L. Braga, X. Liao and A. S. Sant'Ana, *Food Control*, 2021, **132**, 108527.
11 C. B. Penha, E. Bonin, A. Silva, N. Hioka, É. B. Zanqueta, T. U. Nakamura, B. Filho, P. Campanerut-Sá and J. Mikcha, *LWT–Food Sci. Technol.*, 2017, **76**, 198–202.
12 M. Sun, Y. Zhang, Y. He, M. Xiong, H. Huang, S. Pei, J. Liao, Y. Wang and D. Shao, *Colloids Surf., B*, 2019, **180**, 313–318.
13 M. Rai, A. P. Ingle, R. Pandit, P. Paralikar, N. Anasane and C. Santos, *Expert Rev. Anti-Infect. Ther.*, 2020, **18**, 367–379.
14 L. C. Price and R. W. Buescher, *J. Food Sci.*, 1997, **62**, 267–269.
15 B. Wu, J. Fu, Y. Zhou, Y. Shi, J. Wang, X. Feng, Y. Zhao, G. Zhou, C. Lu, G. Quan, X. Pan and C. Wu, *Pharmaceutics*, 2019, **11**, 463.
16 Z. Lei, Q. Tang, Y. Ju, Y. Lin, X. Bai, H. Luo and Z. Tong, *J. Biomater. Sci., Polym. Ed.*, 2020, **31**, 695–711.
17 M. Xu, Y. Hu, W. Ding, F. Li, J. Lin, M. Wu, J. Wu, L. g. Wen, B. Qiu, P. Wei and P. Li, *Biomaterials*, 2020, **258**, 120308.
18 H. Darmani, E. Smadi and S. Bataineh, *J. Med. Microbiol.*, 2020, **69**, 617–624.
19 Y. Zhang, P. Sun, L. Zhang, Z. Wang, F. Wang, K. Dong, Z. Liu, J. Ren and X. Qu, *Adv. Funct. Mater.*, 2019, **29**, 1808591–1808594.
20 M. J. Van Vleet, T. Weng, X. Li and J. R. Schmidt, *Chem. Rev.*, 2018, **118**, 3681–3721.
21 A. Kunwar, A. Barik, R. Pandey and K. I. Priyadarsini, *Biochim. Biophys. Acta*, 2006, **1760**, 1513–1520.
22 Y. Wang, T. Ying, J. Li, Y. Xu, R. Wang, Q. Ke, S. Shen, H. Xu and K. Lin, *Chem. Eng. J.*, 2020, **402**, 126273.
23 M. Zheng, S. Liu, X. Guan and Z. Xie, *ACS Appl. Mater. Interfaces*, 2015, **7**, 22181–22187.
24 Z. Liang, X. Liu, Z. Qin, J. Li, J. Yu, X. He, L. Zhu, H. Fan, Y. Hu, J. Yao, C. Shen, C. Wan, B. Zhang and W. Zhao, *LWT*, 2022, **153**, 112491.
25 Y. Cai, J. Guan, W. Wang, L. Wang, J. Su and L. Fang, *J. Food Sci.*, 2021, **86**, 3550–3562.
26 D. Zheng, C. Huang, H. Huang, Y. Zhao, M. Khan, H. Zhao and L. Huang, *Chem. Biodiversity*, 2020, **17**, e2000171.
27 M. J. Kim and H. G. Yuk, *Appl. Environ. Microbiol.*, 2017, **83**, e02582.
28 Z. Luksiene, *Medicina*, 2003, **39**, 1137–1150.
29 H. Sun, G. Li, X. Nie, H. Shi, P. K. Wong, H. Zhao and T. An, *Environ. Sci. Technol.*, 2014, **48**, 9412–9419.
30 P. K. Samantaray, S. Baloda, G. Madras and S. Bose, *ACS Sustainable Chem. Eng.*, 2019, **7**, 18775–18784.
31 B. Boruah, P. K. Samantaray, G. Madras, J. M. Modak and S. Bose, *Chem. Eng. J.*, 2020, **394**, 124777.
32 X. Gao, H. Wu, Z. Hao, X. Ji, X. Lin, S. Wang and Y. Liu, *Nanoscale*, 2020, **12**, 6489–6497.
33 P. K. Samantaray, G. Madras and S. Bose, *ACS Sustainable Chem. Eng.*, 2019, **7**, 1580–1590.
34 A. Tiwari, A. Singh, N. Garg and J. K. Randhawa, *Sci. Rep.*, 2017, **7**, 12598.
35 J. Wang, M. Zheng and Z. Xie, *J. Colloid Interface Sci.*, 2019, **535**, 84–91.